Scalable and Selective Dispersion of Semiconducting Arc-Discharged Carbon Nanotubes by Dithiafulvalene/Thiophene Copolymers for Thin Film Transistors

Huiliang Wang,[†] Jianguo Mei,[‡] Peng Liu,[§] Kristin Schmidt,[⊥] Gonzalo Jiménez-Osés,[§] Sílvia Osuna,[§] Lei Fang,[‡] Christopher J. Tassone,[⊥] Arjan Pieter Zoombelt,[‡] Anatoliy N. Sokolov,[‡] Kendall N. Houk,[§] Michael F. Toney,[⊥] and Zhenan Bao[‡,*]

[†]Department of Materials Science & Engineering and [‡]Department of Chemical Engineering, Stanford University, Stanford, California 94305, United States, [§]Department of Chemistry and Biochemistry, University of California, Los Angeles, California 90095, United States, and [⊥]Stanford Synchrotron Radiation Lightsource, SLAC National Accelerator Laboratory, Menlo Park, California 94025, United States

ABSTRACT

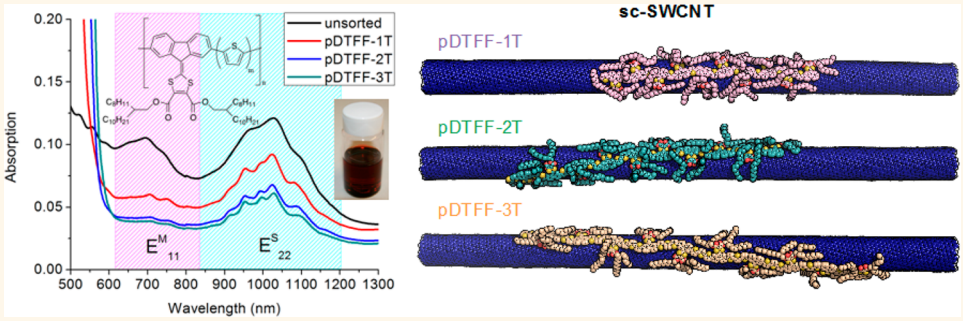

We report a simple and scalable method to enrich large quantities of semiconducting arc-discharged single-walled carbon nanotubes (SWNTs) with diameters of 1.1−1.8 nm using dithiafulvalene/thiophene copolymers. Stable solutions of highly individualized and highly enriched semiconducting SWNTs were obtained after a simple sonication and centrifuge process. Molecular dynamics (MD) simulations of polymer backbone interactions with and without side chains indicated that the presence of long alkyl side chains gave rise to the selectivity toward semiconducting tubes, indicating the importance of the roles of the side chains to both solubilize and confer selectivity to the polymers. We found that, by increasing the ratio of thiophene to dithiafulvalene units in the polymer backbone (from pDTFF-1T to pDTFF-3T), we can slightly improve the selectivity toward semiconducting SWNTs. This is likely due to the more flexible backbone of pDTFF-3T that allows the favorable wrapping of SWNTs with certain chirality as characterized by small-angle X-ray scattering. However, the dispersion yield was reduced from pDTFF-1T to pDTFF-3T. MD simulations showed that the reduction is due to the smaller polymer/SWNT contact area, which reduces the dispersion ability of pDTFF-3T. These experimental and modeling results provide a better understanding for future rational design of polymers for sorting SWNTs. Finally, high on/off ratio solution-processed thin film transistors were fabricated from the sorted SWNTs to confirm the selective dispersion of semiconducting arc-discharge SWNTs.

KEYWORDS: carbon nanotubes · sorting · field-effect transistors · semiconducting

Single-walled carbon nanotubes (SWNTs) have excellent electrical properties for a wide range of applications, such as flexible circuits,[1−4] transparent electrodes,[5−7] sensors,[8,9] and supercapacitors.[10] However, SWNTs are generally produced as a mixture of two-thirds semiconducting and one-third metallic tubes, which prevents their usage in practical electronic applications. Sorting SWNTs *via* solution processing allows the possibility for large-scale sorting using mass-produced, commercial SWNTs and is compatible with procedures used to fabricate low-cost flexible electronic devices.[11−23] While sorting a single-chirality SWNT is important for single-tube-based electronics in order to achieve high device-to-device uniformity, for large-area flexible electronics, a SWNT network is used. Therefore, it is important to

* Address correspondence to zbao@stanford.edu.

Received for review January 4, 2013 and accepted February 12, 2013.

Published online February 12, 2013
10.1021/nn4000435

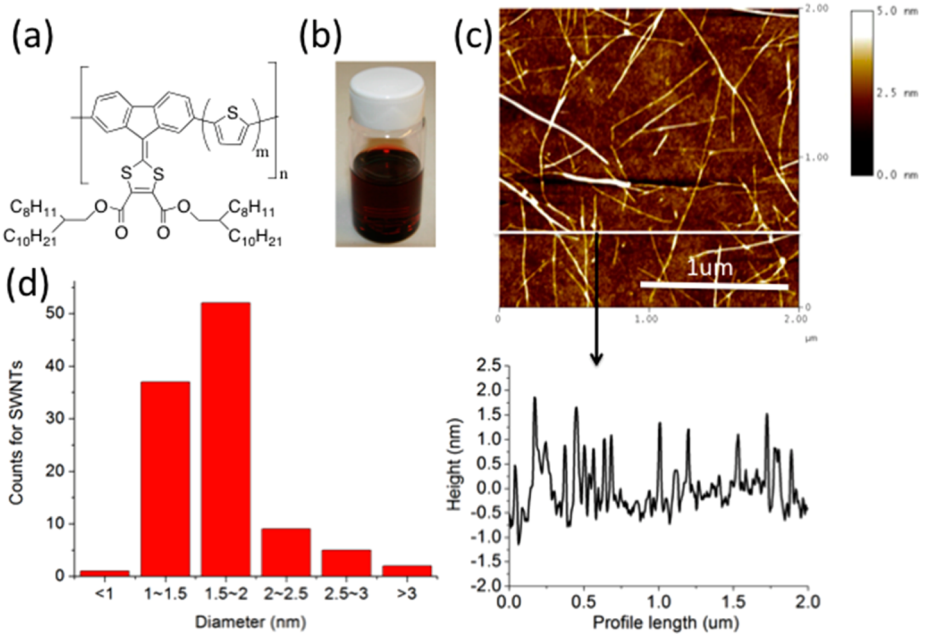

Figure 1. (a) Chemical structure of poly(dithiafulvalene-fluorene-*co*-*m*-thiophene). (b) Picture of a SWNT dispersion obtained from pDTFF-3T polymer in toluene. (c) AFM image of pDTFF-3T-dispersed large-diameter SWNT network and a height line profile to show that SWNTs are all individualized. (d) Height distribution of pDTFF-3T dispersed SWNTs.

enrich high-purity semiconducting SWNTs with a high yield for reduced cost.

We recently reported the dispersion and sorting of small-diameter (0.7−1.1 nm) high-pressure carbon monoxide (HiPco) semiconducting (sc-) SWNTs *via* interaction with polymer semiconductors, regioregular poly(3-alkylthiophene) (rr-P3ATs).[24] The selective dispersion relied on wrapping of SWNTs by the formation of a supramolecular complex with rr-P3ATs. This simple process involves a short sonication followed by centrifugation and is highly selective for semiconducting SWNTs.[24−26] However, the smaller-diameter HiPco tubes are more prone to damage during sonication and generally exhibit a larger Schottky barrier that prevents good electrical contacts.[26,27] Thus, improved separation of larger-diameter (1.1−1.8 nm) arc-discharged SWNTs (AD-SWNTs) is needed. Moreover, AD-SWNTs are generally longer, straighter (Supporting Information Figure S1), and have fewer defects due to decreased wall curvature. This can result in tubes of higher electrical quality that are easier to align than small-diameter tubes. This presents a path to improve performance in electronic applications. The large-diameter SWNTs also allow the insertion of small molecules such as fullerenes to form peapods,[28] a structure suggested for use in quantum computing.[29] Nevertheless, the dispersion and sorting of large-diameter SWNTs has been difficult due to strong van der Waals interactions between the lower curvature walls of the tubes.[30] To date, simple and efficient sorting of large quantities of semiconducting large-diameter SWNTs has not been achieved by polymer wrapping approaches.

Here, we report a facile and efficient process for selective dispersion of a large quantity of semiconducting AD-SWNTs *via* the use of a series of polymers based on poly(dithiafulvalene-fluorene-*co*-*m*-thiophene) (pDTFF-*m*T) (Figure 1a). This method is one of the few methods that can greatly enrich the large-diameter semiconducting SWNTs[12,17,21,31] and can also result in a high yield with such a simple one-step process. Dithiafulvalene (DTF) units are chosen in the polymer because they have large conjugated planar surfaces to form a strong interaction with the SWNT walls as well as the possible interaction through charge transfer.[32,33] By choosing different number of thiophene units (*m*) in the polymer, the polymer conformation and rigidity can be tuned. This will affect the capabilities of each polymer to effectively bind to the wall of the SWNT and hence influence the yield of sorting. In this work, we investigated the dispersion and sorting effects by systematically varying the number of thiophene repeating units in the polymer backbone and fabricated high on/off ratio thin film transistors with the sorted arc-discharged sc-SWNTs.

RESULTS AND DISCUSSION

Sample Preparation and AFM Characterization. The polymers were synthesized using three high yield reactions with an overall yield of up to 60% from inexpensive starting materials (see Methods and Scheme 1). The dispersion process involved sonication of the mixture of polymer/SWNT (1:1 weight ratio) in toluene followed by centrifugation (see Methods). The resulting supernatant was a dark solution, as shown in Figure 1b. Atomic force microscopy was used to characterize the

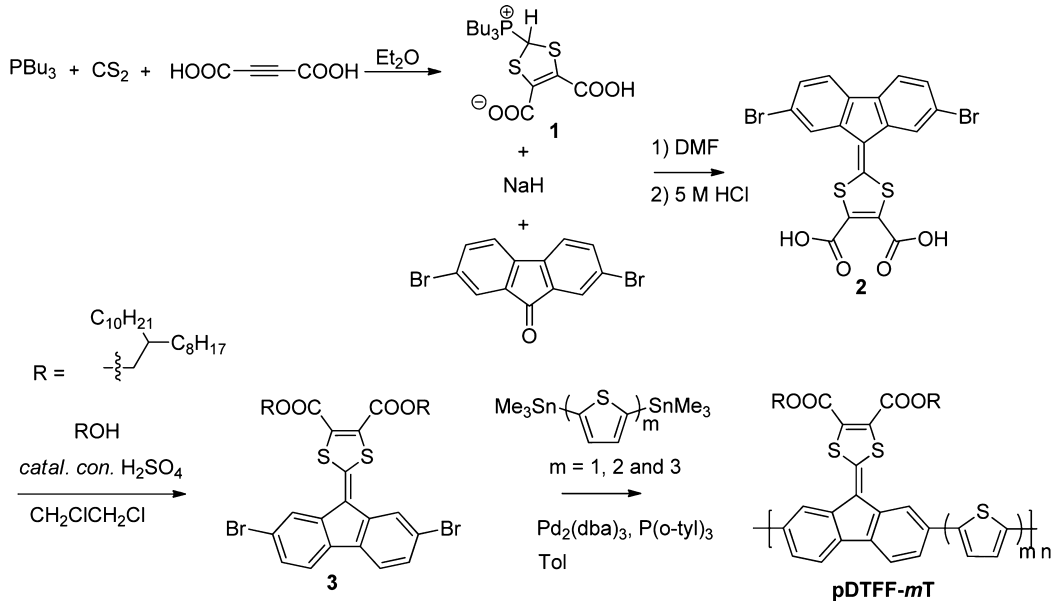

Scheme 1. Synthesis of pDTFF-*m*T

highly individualized nature of SWNTs dispersed by the pDTFF-*m*T (Figure 1c). From the statistics of more than 100 SWNTs, over 85% of the dispersed SWNTs in the AFM line profile exhibited heights of less than 2 nm (Figure 1d), while the average diameter for AD-SWNTs was around 1.4 nm. The slight increase in the height for the dispersed SWNTs is attributed to the polymer on the surface of the SWNTs.

UV—Vis—NIR Characterization. Ultraviolet—visible—near-infrared (UV—vis—NIR) absorption spectroscopy was used to measure the amount of SWNTs dispersed and to estimate the yield of the dispersion process. The polymer-sorted SWNT solutions showed well-resolved peaks in contrast to the broad peak observed for unsorted SWNTs in NMP. This indicates that SWNTs were well-dispersed without large bundles, typically observed as broadened spectrum features. Since the same polymer to SWNT weight ratio and the same amount of solvent were used for preparing the dispersions, the higher absorption peak intensity for pDTFF-1T indicates that it exhibits the highest dispersion efficiency for SWNTs. By comparing the areas of the second interband transition of the semiconducting SWNT (S22) peak between the *N*-methyl-2-pyrrolidone (NMP)-dispersed SWNTs (no sorting, all SWNTs dispersed) and pDTFF-*m*T-sorted SWNTs,[34] the yields for the semiconducting SWNTs were estimated as 44, 32, and 28% for pDTFF-1T, pDTFF-2T, and pDTFF-3T, respectively. The higher dispersion efficiency for pDTFF-1T is attributed to the larger ratio of the DTF derivative to thiophene units in the pDTFF-1T, which results in stronger $\pi-\pi$ interactions with SWNTs, as well as the greater ratio of alkyl side chains, which could also stabilize the polymer/SWNT interactions by C—H$\cdots\pi$ interactions. UV—vis—NIR spectra can also be used to determine the types (metallic or semiconducting) of SWNTs

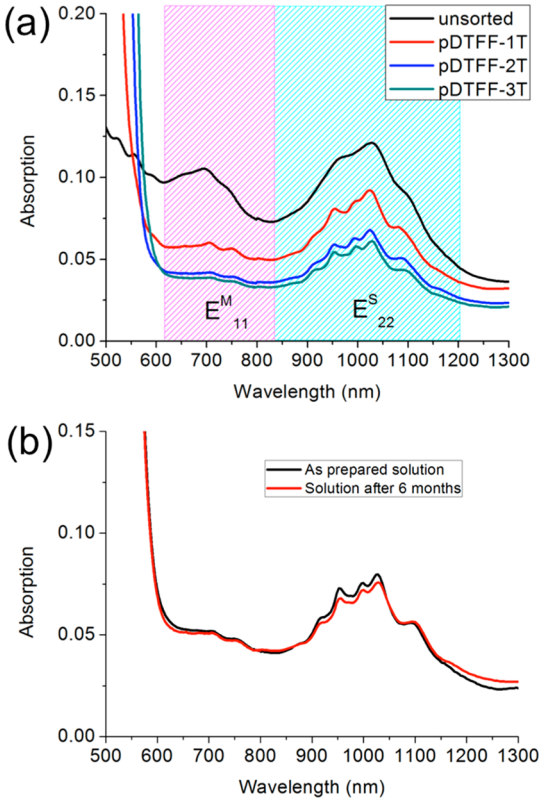

Figure 2. (a) Optical absorption spectrum of carbon nanotubes before and after sorting with pDTFF-*m*T. The unsorted AD-SWNTs were dispersed in *N*-methyl-2-pyrrolidone (NMP). (b) Absorption spectra of the SWNTs dispersed by pDTFF-3T as-prepared and after 6 months.

dispersed by pDTFF-*m*T polymers.[35] For comparison, the semiconducting (S22) peak intensity for unsorted SWNTs dispersed in NMP was normalized to the same intensity as the sorted peak (Figure 2a). Compared to the unsorted AD-SWNTs dispersed in NMP, there was

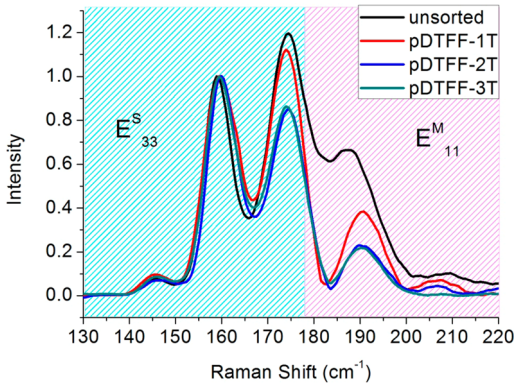

Figure 3. Raman spectrum of unsorted SWNTs dispersed by NMP and sorted SWNTs dispersed by pDTFF-1T, pDTFF-2T, and pDTFF-3T in toluene.

a significant decrease in the first interband transition of metallic SWNT (M11) peaks for polymer-dispersed SWNTs. The M11 peaks for pDTFF-2T and pDTFF-3T are more significantly suppressed compared to that of pDTFF-1T, indicating more selective wrapping of semiconducting SWNTs by these polymers. Since the UV−vis−NIR spectrum shows the absorption from all metallic and semiconducting tubes, comparing the areas under the metallic (M11) and semiconducting peaks (S22) after baseline subtraction,[34] the percentage of semiconducting SWNTs in the sorted tubes can be estimated to be 94% for pDTFF-1T and 96% for both pDTFF-2T and pDTFF-3T. In order to reduce the interference of the polymer peak in the UV−vis−NIR spectra,[24] the polymers were removed by annealing at 500 °C for 1 h in an Ar atmosphere (Figure S2). After normalizing to the semiconducting SWNT (S22) peak, we observed much greater reduction in the M11 peak for the polymer-sorted SWNTs, again indicating an efficient removal of the metallic tubes. The polymer-sorted SWNT dispersion is stable for at least 6 months without visible aggregation or significant reduction/broadening in UV−vis−NIR absorption (Figure 2b).

Raman Characterization. Raman spectroscopy was used to further corroborate the enrichment of semiconducting SWNTs. In order to eliminate the effects of polymers, the supernatant SWNT solution was drop-cast on 300 nm silicon dioxide substrates to make SWNT films. The films were subsequently annealed at 500 °C for 1 h in an Ar atmosphere to remove the polymers before Raman characterization.[24] A laser with 1.96 eV excitation energy was used since it probes peaks from both semiconducting and metallic arc-discharged SWNTs. Other typically available laser sources are 1.58 and 2.33 eV. Unfortunately, they can only probe the semiconducting AD-SWNTs. Therefore, they will not provide information on the effectiveness of removal of metallic SWNTs. The radial breathing modes of both sorted and unsorted SWNTs are shown in Figure 3.[36] The intensities of the spectra are normalized to the peak at 159 cm^{-1}, which represents the semiconducting (16,6) peak so that the relative amount of metallic SWNTs (m-SWNTs) with (11,8) chirality at 189 cm^{-1} can be compared. The polymer-sorted SWNTs showed lower intensity for the metallic peaks than the unsorted ones, demonstrating an enrichment of sc-SWNTs after polymer dispersion. The peak at 192 cm^{-1} is suppressed more significantly for pDTFF-2T and pDTFF-3T than for pDTFF-1T, while the other small peak at 209 cm^{-1} in the metallic region disappeared completely for pDTFF-3T. Therefore, Raman spectroscopy further confirms that pDTFF-*m*T polymers have a preference for enriching sc-SWNTs, with pDTFF-3T showing slightly higher selectivity, consistent with the UV−vis−NIR observations. It is noted that we were unable to make assignments on the chirality using the photoluminescence excitation (PLE) spectrum, which has been commonly used for smaller-diameter tubes, since our large-diameter tubes require a longer wavelength detection that is not readily available for commercial PLE systems. Nevertheless, for thin film SWNT network devices, the sorting of high-purity semiconducting tubes is the most important as the overall device electrical performance will be an average effect of all the tubes present. Using a combination of UV−vis−NIR, Raman, and electrical measurements to be discussed below, we are able to conclude that our sorting process is highly effective in enriching semiconducting SWNTs.

Electrical Characterization. To further confirm the selective sorting of sc-SWNTs, we fabricated thin film transistors (TFTs) of the pDTFF-3T-sorted SWNT network (see Methods). Figure 4a shows the schematic bottom-gate, bottom-contact devices with highly doped Si substrate as a gate and 300 nm SiO_2 as the dielectric layer. The AFM image of the SWNT network between the electrodes is shown in Figure 4b. The transfer and output curves of a representative device are shown in Figure 4c,d, respectively. A charge carrier mobility of 2.8 cm^2/V·s and on/off ratio of 1.6 × 10^4 were obtained with an estimated tube density of 30 SWNTs/μm^2. The best device fabricated by spin-coated pDTFF-3T without SWNTs only gave a mobility of 4 × 10^{-4} cm^2/V·s (Figure S3), confirming that the achieved high mobility came from the SWNT network. Increasing the SWNT network density to ~50 SWNTs/μm^2 resulted in an average mobility up to 20 cm^2/V·s, but a significant reduction in on/off ratio was observed due to the incomplete removal of metallic SWNTs (Figures 4e and S4). For comparison, SWNTs were also dispersed using the same process in pDTFF-3T but with chloroform as the solvent. In this case, the sorting of SWNTs did not happen since the SWNTs have a high solubility in chloroform even in the absence of the polymers. Therefore, this allowed us to prepare unsorted SWNT transistors in the presence of the polymer to show that the observed semiconducting behavior is not a result of polymer−SWNT interaction. The unsorted SWNT transistors were fabricated at the same SWNT density as the sorted ones (Figure S5). From the

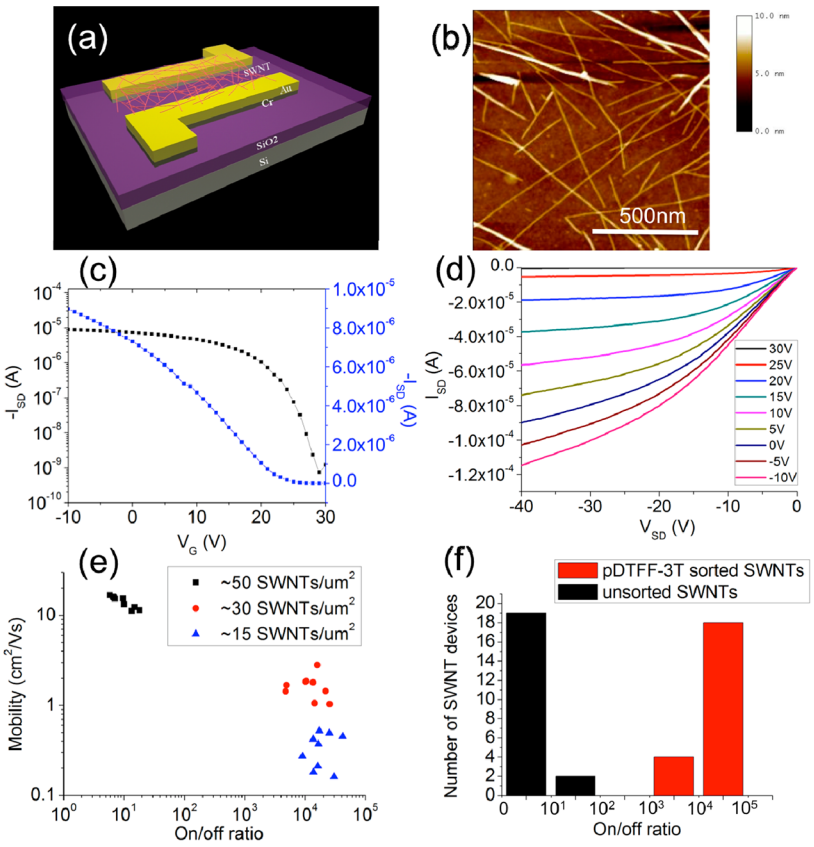

Figure 4. Electrical transport properties of thin film transistors made of pDTFF-3T-dispersed SWNTs in toluene. (a) Schematic diagram of device structure. (b) Morphology of SWNT films of ~30 SWNTs/μm^2. (c) Transfer curve of a typical device ($V_{SD} = -1$ V). (d) Output curves of the device in panel c. (e) Mobility and on/off ratio of pDTFF-3T sorted SWNT transistors at different densities ($V_{SD} = -1$ V). (f) Histogram of on/off ratios for pDTFF-3T-sorted and unsorted SWNT devices of ~30 SWNTs/μm^2.

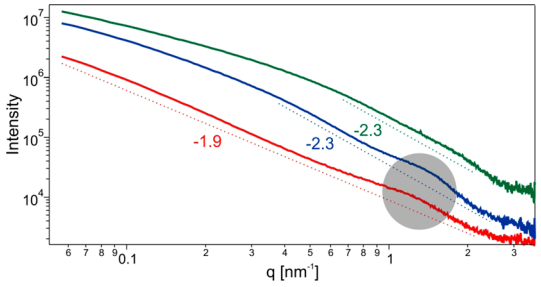

Figure 5. Small-angle X-ray scattering (SAXS) profiles of pDTFF-1T (red), pDTFF-2T (blue), and pDTFF-3T (green) solutions (1 mg/mL dissolved in toluene) as solid lines. The profiles are shifted vertically for better visibility. Dashed lines indicate the linear regime used to extract the Porod exponent. The gray area indicates the broad peak associated with polymer nuclei.

histogram in Figure 4f, we can see that the sorted SWNTs have a significantly improved on/off ratio. The sorted devices have an average on/off ratio of (1.56 ± 1.08) × 10^4 and average mobility of 1.26 ± 0.51 cm^2/V·s, while the unsorted SWNT devices with the same tube density have a very low average on/off ratio of approximately 10, which is attributed to metallic SWNT pathways in the channel. Devices fabricated from pDTFF-1T- and pDTFF-2T-sorted SWNTs at the same density as pDTFF-3T showed slightly lower device performance as compared to pDTFF-3T-sorted ones.

Small-Angle X-ray Scattering (SAXS). In order to understand the selective dispersion of arc-discharged SWNTs observed above, SAXS was performed to determine the polymer conformation in solution and is shown in Figure 5. Previous work on polymer dispersion of SWNTs has attributed the selectivity to the formation of self-assembled molecular structures[18,23] or the energy level matching[21] between SWNTs and the polymers. Here, we hypothesized that the flexibility of the polymer backbone may have an impact on the selectivity of SWNTs. Therefore, SAXS is an ideal technique that allows us to probe the polymer conformation in solution.

The Porod exponent P, obtained from the slope of the scattering profile, gives information about the conformation of the polymer coil. An exponent of $P = 2$ specifies an ideal Gaussian polymer coil, whereas smaller or larger exponents point to extended or collapsed polymer coils, respectively.[37] pDTFF-1T exhibited an exponent of 1.9 over the whole scattering profile, and a Guinier regime could not be observed in the accessible q range. This suggests that the scattering feature is considerably larger than the theoretical value for one polymer chain. Given the fact that the Porod exponent is only slightly smaller than 2, we can assume the formation of a large, loose network structure of the polymer chains. This is probably caused by

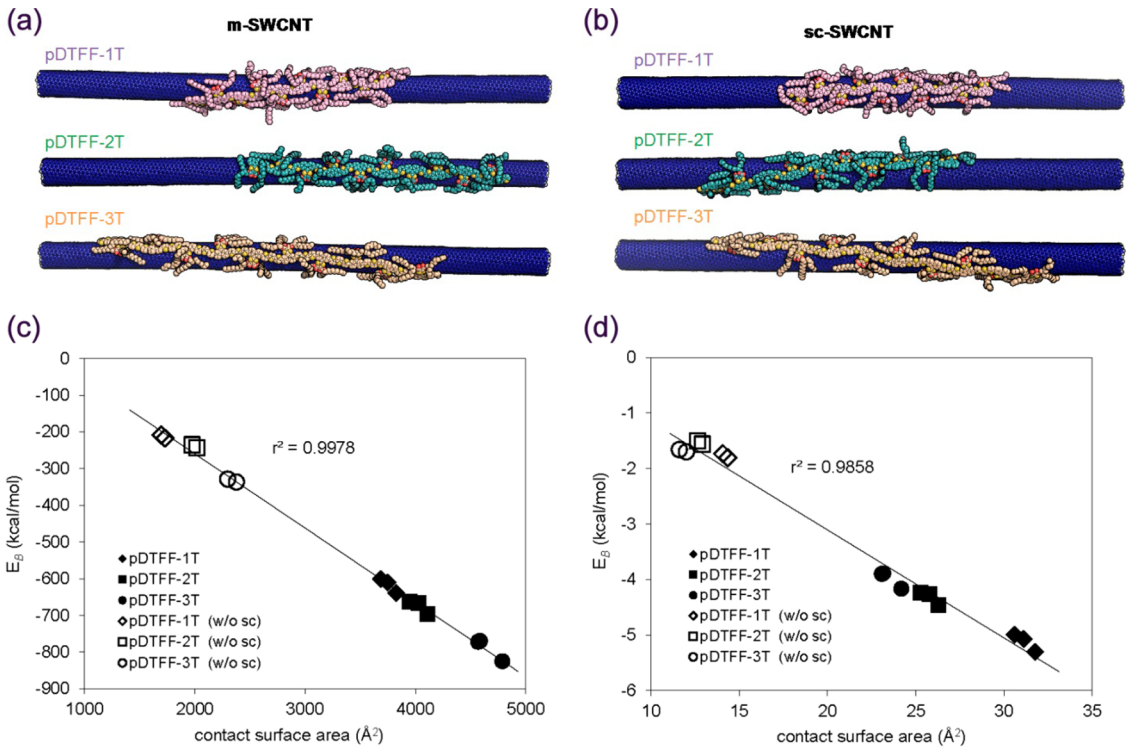

Figure 6. Representative snapshots of the MD simulation for (a) (11,8) m-SWNT and (b) (16,6) sc-SWNT with pDTFF-1T, pDTFF-2T, and pDTFF-3T. Calculated absolute (c) and normalized (d) binding energies (E_B) as a function of the contact surface area (A^2) between the pDTFF-*m*T polymers and both (11,8) m- and (16,6) sc-SWNTs. The computed binding energies and surface areas of polymers without alkyl side chains (labeled as w/o sc) are also shown to illustrate the influence of alkyl side chains. Contact surface areas were averaged along the last 20 ns of 100 ns MD trajectories and were calculated using UCSF Chimera 1.6.

stiffer chain elements that inhibit strong coiling of the polymer chain. This is in contrast to pDTFF-2T and pDTFF-3T, which both show an exponent of 2.3 in the intermediate q range, indicating that these polymers are more collapsed in solution. This suggests that pDTFF-2T and pDTFF-3T are more flexible than pDTFF-1T and are adapting a more coiled structure. The slope change occurring for pDTFF-2T and pDTFF-3T indicates some larger structural features as well as smaller (2−10 nm) ones. In addition, we observed a broad, weak peak at high q vectors for pDTFF-1T and pDTFF-2T, indicating correlations between the polymer chains, which can be interpreted as small, poorly ordered three-dimensional nuclei. The peak shifts slightly to higher q vectors for pDTFF-2T compared to pDTFF-1T, suggesting that the pDTFF-1T nuclei are packed more densely. We expect that this nucleation takes place due to the packing of stiff elements in the polymer chain. Given the observations above, we conclude that pDTFF-3T is the most flexible chain (no sign of nucleation, coiled structure), followed by pDTFF-2T (some nucleation and coiled structure) and pDTFF-1T (some nucleation and more extended structure). The more flexible polymer backbone can potentially allow the polymer to adapt the specific conformation needed to wrap certain chirality of SWNTs and hence may potentially give rise to the increase in selectivity from pDTFF-1T to pDTFF-3T.

Molecular Dynamics (MD) Simulations. To investigate the wrapping geometry of the polymer−SWNT complexes[38−41] and further understand the selectivity achieved with different polymers, MD simulations of the wrapping process were performed in implicit toluene solvent (ε = 2.84) (see Methods). Two representative SWNTs observed by Raman spectroscopy, the metallic (11,8) SWNT and the semiconducting (16,6) SWNT, and three polymers (pDTFF-*m*T, m = 1−3) were used in the modeling.

During the very initial stages of the 100 ns simulation, the polymer backbones gradually evolved from a linear arrangement in the initial structure to a more helical wrapping around the circumference of the tube (see Supporting Information for movies of the initial wrapping process). Eventually, after approximately 200 ps, the polymer backbone subsequently extended to a more stable quasi-linear conformation and remained in contact with the nanotube surface (see movies in the Supporting Information and the representative snapshots in Figure 6a,b). Previous MD studies by Grossman[39] and Mattoni[38] groups indicated similar phenomena in the wrapping process of polythiophene with the SWNT. This final linear conformation is reproduced regardless of the starting orientation of the polymer with respect to the SWNT. Most alkyl side chains also remained bound to the nanotube surface during the 100 ns simulations. Snapshots of the structures of the polymers interaction with metallic

TABLE 1. Average Binding Energies of Polymers pDTFF-*m*T (a) with Side Chain and (b) without Side Chain with (11,8) and (16,6) SWNTs[a]

		absolute binding energies			normalized binding energies		
(a)	length (Å)	(11,8) m-SWNT	(16,6) sc-SWNT	ΔE_B	(11,8) m-SWNT	(16,6) sc-SWNT	ΔE_B
pDTFF-1T	120.5	−600.4	−634.4	−34.0	−5.0	−5.3	−0.3
pDTFF-2T	156.3	−652.1	−681.6	−29.5	−4.2	−4.4	−0.2
pDTFF-3T	198.0	−765.7	−823.3	−57.6	−3.9	−4.2	−0.3
		absolute binding energies			normalized binding energies		
(b)	length (Å)	(11,8) m-SWNT	(16,6) sc-SWNT	ΔE_B	(11,8) m-SWNT	(16,6) sc-SWNT	ΔE_B
pDTFF-1T (w/o sc)	120.5	−209.1	−217.4	−8.3	−1.7	−1.8	−0.1
pDTFF-2T (w/o sc)	156.3	−235.1	−244.0	−8.9	−1.5	−1.6	−0.1
pDTFF-3T (w/o sc)	198.0	−328.7	−336.7	−8.0	−1.7	−1.7	0.0

[a] Average binding energies computed from the last 20 ns of simulation. Absolute energies are in kcal/mol, and normalized energies are in kcal/mol^{-1}Å^{-1}.

and semiconducting SWNTs obtained after 60 ns simulation are shown in Figure 6a,b, respectively.

We computed the normalized binding energy (E_B) of the SWNT/pDTFF-*m*T complex as $E_B = [E_{complex} - (E_{SWNT} + E_{pDTFF\text{-}mT})/l_{pDTFF\text{-}mT}$, where $E_{complex}$, E_{SWNT}, and $E_{pDTFF\text{-}mT}$ are the energies of the SWNT/pDTFF-*m*T complex, the nanotube, and the polymer, respectively, based on the implicit generalized Born (GB) solvation model,[42] and $l_{pDTFF\text{-}mT}$ is the length of the polymer in an idealized extended conformation (in Å). The binding energies of our polymers with metallic and semiconducting SWNTs are shown in Table 1. Interestingly, all three polymers exhibit stronger binding to the semiconducting nanotube than to the metallic one. This is attributed to the more planar surface of the larger-diameter (16,6) semiconducting nanotube, which interacts more preferably with the polymer backbone and side chains. Within the last 20 ns of simulation, when the systems are completely equilibrated, the average normalized binding energies of pDTFF-1T with both (16,6) sc-SWNT and (11,8) m-SWNT are the greatest among the three polymers (−5.3 and −5.0 mol^{-1}Å^{-1}, respectively), and the binding energies of pDTFF-2T (−4.4 and −4.2 mol^{-1}Å^{-1}) are slightly larger than those of pDTFF-3T (−4.2 and −3.9 mol^{-1}Å^{-1}), in agreement with the measured amounts of SWNTs dispersed. A possible explanation is that the greater number of side chains per length unit in pDTFF-1T leads to higher surface contact area for the same length of polymer and thus gives rise to higher binding energies with the nanotubes. The computed binding energies are in good linear relationship with the surface contact area (Figure 6c,d). On the other hand, the difference in computed selectivity of different polymer is rather small (0.2−0.3 mol^{-1}Å^{-1}), even though in qualitative agreement with the trend observed experimentally. Interestingly, when the same MD simulations were performed using only the polymer backbones without the side chains (*i.e.*, the alkyl side chains were replaced with H atoms), the binding energies between the three polymers with the semiconducting and metallic SWNTs were all similar and the computed selectivities between semiconducting and metallic SWNTs were diminished (Table 1b). This suggests that the side chains promote polymer/SWNT binding and can also contribute to the observed selectivity.

CONCLUSION

In summary, we synthesized a new series of polymers (pDTFF-*m*T) that selectively dispersed large-diameter arc-discharged semiconducting SWNTs in high yields by a simple sonication and centrifugation process. We found that the amounts of SWNTs dispersed were proportional to the available contact areas from the polymers, and the increased polymer flexibility tends to improve selectivity. Spectroscopic characterizations by UV−vis−NIR and Raman confirm the selectivity for semiconducting SWNTs. Additionally, thin film transistors showed on/off ratios greater than 10^4 from pDTFF-3T-sorted SWNTs. The sorted, concentrated, and stable large-diameter semiconducting SWNT solutions have great potential for applications in thin film TFTs, sensors, and as the semiconducting active layer in solar cells.

METHODS

Materials and Characterizations. All reagents and starting materials were purchased from commercial sources and used without further purification, unless otherwise noted. ^{1}H and ^{13}C NMR spectra were recorded using Varian Inova 500 in deuterated chloroform at 293 K. Mass spectrograms were recorded on either a Finnigan MAT95Q Hybrid Sector (EI, HRMS) or a Bruker Reflex II (MALDI-TOF) mass spectrometer operated in linear mode with delayed extraction at University of Florida. Elemental

analyses were carried out by Robertson Microlit. Size exclusion chromatography (SEC) was performed in THF solution, and the molecular weights were calculated using a calibration curve based on polystyrene standards. Thermal gravimetric analyses (TGA) were performed using a Mettler Toledo TGA/SDTA 851e at a heating rate of 10 °C min^{-1} under a nitrogen flow (20 mL/min).

5-Carboxy-2-(tributylphosphonio)-1,3-dithiole-4-carboxylate (1). This compound was prepared according to the literature procedure [*Chem. Commun*, **1975**, *24*, 960].

2-(2,7-Dibromo-9*H*-fluoren-9-ylidene)-1,3-dithiole-4,5-dicarboxylic acid (2). Compound **1** (3.1 g, 7.87 mmol) and commercially available 2,7-dibromo-9*H*-fluoren-9-one (2.5 g, 7.5 mmol) were dissolved into anhydrous DMF (80 mL) and stirred for 10 min. NaH (0.9 g, 60 wt %) was added under inert atmosphere. Yellow-orange precipitate was formed over the time. After 10 h, the suspension was sonicated for another 10 min and then poured into methanol (500 mL). The precipitates were collected by vacuum filtration, washed with methanol, and dried in the air. The yellow sodium salts were then suspended into distilled water (1g/2L), and the suspension was stirred for 3 h until all of the solids disappeared (insoluble portion was filtered and discarded), followed by the addition of HCl (5 M, 20 mL). The solution immediately turned deep red. The acids were extracted with a mixture of chloroform and isopropyl alcohol (1 g/600 mL; v/v = 1:2). The obtained organic phase, without drying, was concentrated under rotovap and then poured into cold methanol (1 g/150 mL). The deep red precipitates were collected *via* vacuum filtration, dried in the air, and then stored under high vacuum for 20 h to give 3.4 g of a red solid (87%). ^{1}H NMR (DMSO, 400 Hz) δ: 7.80 (d, J = 8 Hz, 2H), 7.49 (d, J_1 = 1.6 Hz, 2H), 7.41 (d, J_1 = 1.6 Hz, J_2 = 8 Hz, 2H). ^{13}C NMR (DMSO, 400 Hz) δ: 160.2, 139.6, 138.2, 137.5, 134.8, 127.8, 124.5, 121.8, 120.4, 115.7.

Bis(2-octyldodecyl)-2-(2,7-dibromo-9*H*-fluoren-9-ylidene)-1,3-dithiole-4,5-dicarboxylate (3). To a solution of 2-(2,7-dibromo-9*H*-fluoren-9-ylidene)-1,3-dithiole-4,5-dicarboxylic acid (3 mmol) and branched alcohol (30 equiv) in CH_2ClCH_2Cl (40 mL) was added concentrated sulfuric acid (3 mL) through a pipet. Inside the flask, a thimble filled with 4 Å molecular sieves was attached onto the septum. The deep red suspension was heated to reflux (83 °C) and stirred 20 h. Upon being cooled to room temperature, the clear orange-red solution was poured into distilled water (300 mL). The organic layer was extracted with CH_2Cl_2 and washed with saturated $NaHCO_3$ (1 × 50 mL). The combined organic phase was dried with magnesium sulfate and concentrated under vacuum. The resulting sticky red oil was purified by silica gel chromatography, eluting with hexane/ethyl acetate (95:5).

Yield: 2.87 g (81%). ^{1}H NMR ($CDCl_3$, 400 Hz) δ: 7.72 (d, J = 1.6 Hz, 2H), 7.59 (d, J = 8 Hz, 2H), 7.43 (d, J_1 = 1.6 Hz, J_2 = 8 Hz, 2H), 4.27 (d, J = 6 Hz, 4H), 1.79−1.76 (m, 2H), 1.39−1.20 (m, 64H), 0.90−0.82 (m, 12H). ^{13}C NMR ($CDCl_3$ 400 Hz) δ: 159.2, 138.1, 132.1, 129.1, 126.1, 121.4, 121.1, 119.2, 70.4, 37.5, 37.3, 32.2, 31.8, 31.4, 30.2, 30.0, 29.9, 29.6(3), 29.6(2), 27.3, 27.0, 22.9, 14.4. HRMS (ESI-TOF) calcd for $C_{58}H_{88}Br_2O_4S_2$ $(M + H)^+$: 1073.4556, found *m/z* 1073.4530. Anal. Calcd for $C_{58}H_{88}Br_2O_4S_2$: C, 64.91; H, 8.59. Found: C, 67.19; H, 8.59.

General Procedure for Polymerization. To a microwave vessel (8 mL) charged with a string bar, equal mole of (Th)m$(SnMe_3)_2$ (0.5 mmol) and compound **3** (0.25 mmol) was added, followed by the addition of degassed toluene (6 mL). The resulting solution was bubbled with argon for 15 min. $Pd_2(dba)_3$ (16 mg) and P(o-tyl)$_3$ (9 mg) were quickly added under argon. The vessel was then sealed with a snap cap, purged with argon for 5 min, and subjected to the following reaction conditions in a microwave reactor (Microwave Setups: CEM Discover Automatic Microwave Reactor; power cycling; power = 300 W; power cycles = 40; temperature = 125−185 °C; heating = 150 s; cooling = 30 s; pressure = 150 psi; stirring = high). After the completion, the reaction was automatically cooled to room temperature and the obtained solids were suspended into acetone. The solids were collected by filtration through a high-quality glass thimble. The thimble was left inside a Soxhlet extractor, and the solids were successively extracted with acetone, hexane, and chloroform. The chloroform fraction was concentrated and precipitated into acetone. The polymer was filtered and dried *in vacuo* at 60 °C overnight. pDTFF-1T: 348 mg (90%), M_n = 32 kDa, PDI = 1.2. pDTFF-2T: 446 mg (92%), M_n = 84 kDa, PDI = 1.9. pDTFF-3T: 399 mg (67%), M_n = 50 kDa, PDI = 2.1. The molecular weight and PDI of the polymers are summarized in Table S1.

Preparation of SWNT Solution. Four milligrams of pDTFF-*m*T and 3 mg of arc-discharge SWNTs were mixed in 25 mL of toluene and sonicated (Cole Parmer ultrasonic processor 750 W) for 30 min at an amplitude level of 70%. The solution was then centrifuged (Sorvall RC5C-plus) at 17 000 rpm for 1 h at 16 °C. The supernatants were collected and diluted to 1:100 with toluene before making devices. Then, 3 mg of SWNTs was also sonicated in 25 mL of NMP for UV−vis−NIR measurements to compare the yields of polymer sorting.

SWNT Structure Characterization. AFM images were taken using tapping mode with a Veeco AFM. Electrical measurements were done using a Keithley 4200 SC semiconductor analyzer. Raman spectral analysis was performed on a confocal Raman system LabRam Aramis from Horiba Jobin Yvon at 633 nm (1.96 eV) excitation at 100× magnification, 1 μm spot size, 1800 grating, and 5 mV excitation power. Data were taken by as an average of multiple points mapping (9 points) for two substrates. Each point is an average of three spectra. The spectrum was normalized to the 521 cm^{-1} silicon peak. The UV−vis−NIR measurements were done in 1 mm path-length quartz cells by using a Cary 6000i spectrophotometer (Varian) with toluene as a background.

Polymer SAXS Measurement. The scattering experiments were carried out at beamline 4-2 at the Stanford Synchrotron Radiation Lightsource. The measurements were performed with a 14 keV X-ray energy beam with a size of 0.2 × 0.8 mm. The scattering data were collected with a 2D CCD detector (Rayonix MX 225HE) at a distance of 3.5 m from the sample. The polymer concentration was 1 mg/mL in toluene to improve the contrast of the polymer to solvent scattering. We performed scattering experiments at 0.2 mg/mL as well to ensure that these solutions exhibit the same structural features (shown in Figure S6). The data were masked, normalized, and integrated using SAXS programs written by Bösecke.[43] After background subtraction of the pure solvent scattering, the scattering profiles were fitted using a combination of Porod's and Guinier's law as described elsewhere.[44]

Molecular Dynamics Simulations. The simulations were performed in implicit toluene solvent (ε = 2.84) using AMBER 11 and the general AMBER force field (GAFF). The partial charges sets were obtained by fitting the electrostatic potential generated at the HF/6-31G(d) level by the RESP model. The partial charges of the nanotube carbon atoms were set to zero. A 30 nm long nanotube and a polymer with 10 repeating units (n = 10) were employed in each simulation. The starting structures for the MD simulations consisted of the planar configuration of the three polymers situated *ca.* 5 Å from the nanotube surface at an angle of *ca.* 45° with respect to the nanotube (Figure S7).

Device Fabrication and Electrical Characterization. The drain and source electrodes for bottom-contact device electrodes were fabricated on a highly doped 4 in. silicon wafer with 300 nm SiO_2 by photolithography. A bilayer of Cr (5 nm) and Au (40 nm) was deposited by thermal evaporation as the source−drain electrodes, followed by a lift-off process in acetone. The substrate was then soaked in the (1:100 ratio) diluted solution of sorted SWNTs for 2 h. A Keithley 4,200 SC semiconductor analyzer was used to measure the electrical properties of the devices. Source−drain voltage (V_{SD}) of −1 V was used for all of the reported measurements.

Conflict of Interest: The authors declare no competing financial interest.

Acknowledgment. This work was funded by National Science Foundation (ECCS 0901414 and Award No. 1059020 to Z.B.; CHE-1059084 to K.N.H.), and Global Climate and Energy Project (GCEP) at Stanford University. H.W. acknowledges financial support from Link Foundation Energy fellowship. S.O. acknowledges the European Community for the postdoctoral fellowship PIOF-GA-2009-252856, G.J.-O. acknowledges the Ministerio de Educación for the postdoctoral fellowship (EX2010-1063). We thank Jeff Han, Do Hwan Kim, Chao Wang,

Steve Park, Satoshi Morishita, and T. M. Weiss for assistance in both experimental works and discussion. Scattering experiments were carried out at beamline 4-2 of the Stanford Synchrotron Radiation Lightsource. The SSRL Structural Molecular Biology Program is supported by the DOE Office of Biological and Environmental Research, and by the National Institutes of Health.

Supporting Information Available: Supporting figures (Figures S1−S7) and movies of the MD simulations. This material is available free of charge *via* the Internet at http://pubs.acs.org.

REFERENCES AND NOTES

1. Cao, Q.; Kim, H. S.; Pimparkar, N.; Kulkarni, J. P.; Wang, C.; Shim, M.; Roy, K.; Alam, M. A.; Rogers, J. A. Medium-Scale Carbon Nanotube Thin-Film Integrated Circuits on Flexible Plastic Substrates. *Nature* **2008**, *454*, 495–500.
2. Gruner, G. Carbon Nanotube Films for Transparent and Plastic Electronics. *J. Mater. Chem.* **2006**, *16*, 3533–3539.
3. Rouhi, N.; Jain, D.; Burke, P. J. High-Performance Semiconducting Nanotube Inks: Progress and Prospects. *ACS Nano* **2011**, *5*, 8471–8487.
4. Wang, C.; Chien, J.-C.; Takei, K.; Takahashi, T.; Nah, J.; Niknejad, A. M.; Javey, A. Extremely Bendable, High-Performance Integrated Circuits Using Semiconducting Carbon Nanotube Networks for Digital, Analog, and Radio-Frequency Applications. *Nano Lett.* **2012**, *12*, 1527–1533.
5. Zhang, D.; Ryu, K.; Liu, X.; Polikarpov, E.; Ly, J.; Tompson, M. E.; Zhou, C. Transparent, Conductive, and Flexible Carbon Nanotube Films and Their Application in Organic Light-Emitting Diodes. *Nano Lett.* **2006**, *6*, 1880–1886.
6. Hu, L.; Hecht, D. S.; Gruner, G. Carbon Nanotube Thin Films: Fabrication, Properties, and Applications. *Chem. Rev.* **2010**, *110*, 5790–5844.
7. Hellstrom, S. L.; Lee, H. W.; Bao, Z. Polymer-Assisted Direct Deposition of Uniform Carbon Nanotube Bundle Networks for High Performance Transparent Electrodes. *ACS Nano* **2009**, *3*, 1423–1430.
8. Roberts, M. E.; LeMieux, M. C.; Bao, Z. Sorted and Aligned Single-Walled Carbon Nanotube Networks for Transistor-Based Aqueous Chemical Sensors. *ACS Nano* **2009**, *3*, 3287–3293.
9. Chen, R. J.; Choi, H. C.; Bangsaruntip, S.; Yenilmez, E.; Tang, X.; Wang, Q.; Chang, Y. L.; Dai, H. An Investigation of the Mechanisms of Electronic Sensing of Protein Adsorption on Carbon Nanotube Devices. *J. Am. Chem. Soc.* **2004**, *126*, 1563–1568.
10. Futaba, D. N.; Hata, K.; Yamada, T.; Hiraoka, T.; Hayamizu, Y.; Kakudate, Y.; Tanaike, O.; Hatori, H.; Yumura, M.; Iijima, S. Shape-Engineerable and Highly Densely Packed Single-Walled Carbon Nanotubes and Their Application as Supercapacitor Electrodes. *Nat. Mater.* **2006**, *5*, 987–994.
11. Artukovic, E.; Kaempgen, M.; Hecht, D. S.; Roth, S.; Grüner, G. Transparent and Flexible Carbon Nanotube Transistors. *Nano Lett.* **2005**, *5*, 757–760.
12. Arnold, M. S.; Green, A. A.; Hulvat, J. F.; Stupp, S. I.; Hersam, M. C. Sorting Carbon Nanotubes by Electronic Structure Using Density Differentiation. *Nat. Nanotechnol.* **2006**, *1*, 60–65.
13. Ghosh, S.; Bachilo, S. M.; Weisman, R. B. Advanced Sorting of Single-Walled Carbon Nanotubes by Nonlinear Density-Gradient Ultracentrifugation. *Nat. Nanotechnol.* **2010**, *5*, 443–450.
14. Tu, X.; Manohar, S.; Jagota, A.; Zheng, M. DNA Sequence Motifs for Structure-Specific Recognition and Separation of Carbon Nanotubes. *Nature* **2009**, *460*, 250–253.
15. Zheng, M.; Jagota, A.; Strano, M. S.; Santos, A. P.; Barone, P.; Chou, S. G.; Diner, B. A.; Dresselhaus, M. S.; McLean, R. S.; Onoa, G. B; *et al.* Structure-Based Carbon Nanotube Sorting by Sequence-Dependent DNA Assembly. *Science* **2003**, *302*, 1545–1548.
16. Liu, H.; Nishide, D.; Tanaka, T.; Kataura, H. Large-Scale Single-Chirality Separation of Single-Wall Carbon Nanotubes by Simple Gel Chromatography. *Nat. Commun.* **2011**, *2*, 309.
17. Tanaka, T.; Jin, H.; Miyata, Y.; Fujii, S.; Suga, H.; Naitoh, Y.; Minari, T.; Miyadera, T.; Tsukagoshi, K.; Kataura, H. Simple and Scalable Gel-Based Separation of Metallic and Semiconducting Carbon Nanotubes. *Nano Lett.* **2009**, *9*, 1497–1500.
18. Nish, A.; Hwang, J. Y.; Doig, J.; Nicholas, R. J. Highly Selective Dispersion of Single-Walled Carbon Nanotubes Using Aromatic Polymers. *Nat. Nanotechnol.* **2007**, *2*, 640–646.
19. Voggu, R.; Rao, K. V.; George, S. J.; Rao, C. N. R. A Simple Method of Separating Metallic and Semiconducting Single-Walled Carbon Nanotubes Based on Molecular Charge Transfer. *J. Am. Chem. Soc.* **2010**, *132*, 5560–5561.
20. Qiu, H.; Maeda, Y.; Akasaka, T. Facile and Scalable Route for Highly Efficient Enrichment of Semiconducting Single-Walled Carbon Nanotubes. *J. Am. Chem. Soc.* **2009**, *131*, 16529–16533.
21. Tange, M.; Okazaki, T.; Iijima, S. Selective Extraction of Large-Diameter Single-Wall Carbon Nanotubes with Specific Chiral Indices by Poly(9,9-dioctylfluorene-*alt*-benzothiadiazole). *J. Am. Chem. Soc.* **2011**, *133*, 11908–11911.
22. Zhang, H.; Wu, B.; Hu, W.; Liu, Y. Separation and/or Selective Enrichment of Single-Walled Carbon Nanotubes Based on Their Electronic Properties. *Chem. Soc. Rev.* **2011**, *40*, 1324–1336.
23. Chen, F.; Wang, B.; Chen, Y.; Li, L.-J. Toward the Extraction of Single Species of Single-Walled Carbon Nanotubes Using Fluorene-Based Polymers. *Nano Lett.* **2007**, *7*, 3013–3017.
24. Lee, H. W.; Yoon, Y.; Park, S.; Oh, J. H.; Hong, S.; Liyanage, L. S.; Wang, H.; Morishita, S.; Patil, N.; Park, Y. J.; *et al.* Selective Dispersion of High Purity Semiconducting Single-Walled Carbon Nanotubes with Regioregular Poly(3-alkylthiophene)s. *Nat. Commun.* **2011**, *2*, 541.
25. Liyanage, L. S.; Lee, H.; Patil, N.; Park, S.; Mitra, S.; Bao, Z.; Wong, H.-S. P. Wafer-Scale Fabrication and Characterization of Thin-Film Transistors with Polythiophene-Sorted Semiconducting Carbon Nanotube Networks. *ACS Nano* **2011**, *6*, 451–458.
26. Park, S.; Lee, H. W.; Wang, H.; Selvarasah, S.; Dokmeci, M. R.; Park, Y. J.; Cha, S. N.; Kim, J. M.; Bao, Z. Highly Effective Separation of Semiconducting Carbon Nanotubes Verified *via* Short-Channel Devices Fabricated Using Dip-Pen Nanolithography. *ACS Nano* **2012**, *6*, 2487–2496.
27. Kim, W.; Javey, A.; Tu, R.; Cao, J.; Wang, Q.; Dai, H. Electrical Contacts to Carbon Nanotubes Down to 1 nm in Diameter. *Appl. Phys. Lett.* **2005**, *87*, 1–3.
28. Okada, S.; Saito, S.; Oshiyama, A. Energetics and Electronic Structures of Encapsulated C_{60} in a Carbon Nanotube. *Phys. Rev. Lett.* **2001**, *86*, 3835–3838.
29. Ge, L.; Montanari, B.; Jefferson, J. H.; Pettifor, D. G.; Harrison, N. M.; Briggs, G. A. D. Modeling Spin Interactions in Carbon Peapods Using a Hybrid Density Functional Theory. *Phys. Rev. B* **2008**, *77*, 235416.
30. Tersoff, J.; Ruoff, R. S. Structural Properties of a Carbon-Nanotube Crystal. *Phy. Rev. Lett.* **1994**, *73*, 676–679.
31. Berton, N.; Lemasson, F.; Tittmann, J.; Stürzl, N.; Hennrich, F.; Kappes, M. M.; Mayor, M. Copolymer-Controlled Diameter-Selective Dispersion of Semiconducting Single-Walled Carbon Nanotubes. *Chem. Mater.* **2011**, *23*, 2237–2249.
32. Voggu, R.; Rout, C. S.; Franklin, A. D.; Fisher, T. S.; Rao, C. N. R. Extraordinary Sensitivity of the Electronic Structure and Properties of Single-Walled Carbon Nanotubes to Molecular Charge-Transfer. *J. Phys. Chem. C* **2008**, *112*, 13053–13056.
33. Varghese, N.; Ghosh, A.; Voggu, R.; Ghosh, S.; Rao, C. N. R. Selectivity in the Interaction of Electron Donor and Acceptor Molecules with Graphene and Single-Walled Carbon Nanotubes. *J. Phys. Chem. C* **2009**, *113*, 16855–16859.
34. Tan, Y.; Resasco, D. E. Dispersion of Single-Walled Carbon Nanotubes of Narrow Diameter Distribution. *J. Phys. Chem. B* **2005**, *109*, 14454–14460.

35. Kang, Y. K.; Lee, O. S.; Deria, P.; Kim, S. H.; Park, T. H.; Bonnell, D. A.; Saven, J. G.; Therien, M. J. Helical Wrapping of Single-Walled Carbon Nanotubes by Water Soluble Poly-(*p*-phenyleneethynylene). *Nano Lett.* **2009**, *9*, 1414–1418.
36. Dresselhaus, M. S.; Dresselhaus, G.; Jorio, A.; Souza Filho, A. G.; Saito, R. Raman Spectroscopy on Isolated Single Wall Carbon Nanotubes. *Carbon* **2002**, *40*, 2043–2061.
37. Beaucage, G. Small-Angle Scattering from Polymeric Mass Fractals of Arbitrary Mass-Fractal Dimension. *J. Appl. Crystallogr.* **1996**, *29*, 134–146.
38. Caddeo, C.; Melis, C.; Colombo, L.; Mattoni, A. Understanding the Helical Wrapping of Poly(3-hexylthiophene) on Carbon Nanotubes. *J. Phys. Chem. C* **2010**, *114*, 21109–21113.
39. Bernardi, M.; Giulianini, M.; Grossman, J. C. Self-Assembly and Its Impact on Interfacial Charge Transfer in Carbon Nanotube/P3HT Solar Cells. *ACS Nano* **2010**, *4*, 6599–6606.
40. Lemasson, F. A.; Strunk, T.; Gerstel, P.; Hennrich, F.; Lebedkin, S.; Barner-Kowollik, C.; Wenzel, W.; Kappes, M. M.; Mayor, M. Selective Dispersion of Single-Walled Carbon Nanotubes with Specific Chiral Indices by Poly(*N*-decyl-2,7-carbazole). *J. Am. Chem. Soc.* **2010**, *133*, 652–655.
41. Ozawa, H.; Fujigaya, T.; Niidome, Y.; Hotta, N.; Fujiki, M.; Nakashima, N. Rational Concept To Recognize/Extract Single-Walled Carbon Nanotubes with a Specific Chirality. *J. Am. Chem. Soc.* **2011**, *133*, 2651–2657.
42. Tsui, V.; Case, D. A. Theory and Applications of the Generalized Born Solvation Model in Macromolecular Simulations. *Biopolymers* **2001**, *56*, 275–291.
43. Boesecke, P. Reduction of Two-Dimensional Small- and Wide Angle X-ray Scattering Data. *J. Appl. Crystallogr.* **2007**, *40*, S423–S427.
44. Hammouda, B. A New Guinier−Porod Model. *J. Appl. Crystallogr.* **2010**, *43*, 716–719.